ACS APPLIED MATERIALS & INTERFACES

Research Article

www.acsami.org

Tin Oxide Nanosheet Assembly for Hydrophobic/Hydrophilic Coating and Cancer Sensing

Yoshitake Masuda,* Tatsuki Ohji, and Kazumi Kato

National Institute of Advanced Industrial Science and Technology (AIST), 2266-98 Anagahora, Shimoshidami, Moriyama-ku, Nagoya 463-8560, Japan

Supporting Information

ABSTRACT: Tin oxide nanosheets were crystallized on transparent conductive oxide substrates of fluorine-doped tin oxide in aqueous solutions. The nanosheets had chemical ratio of Sn:O:F = 1:1.85:0.076, suggesting fluorine doping into SnO_2. They were hydrophobic surfaces with contact angle of 140°. They were converted to hydrophilic surfaces with contact angle of below 1° by light irradiation. The simple water process will be applied to surface coating of polymers, metals, biomaterials, papers, etc. Furthermore, the tin oxide nanosheets were modified with dye-labeled monoclonal antibody. Monoclonal antibody reacts with human alpha-fetoprotein in blood serum of hepatocellular cancer patient. Photoluminescence and photocurrent were obtained from the nanosheets under excitation light. Photoelectric conversion was an essence in the sensing system. The tin oxide nanosheets with dye-labeled prostate specific antigen will be used for electrodes of prostate cancer sensors.

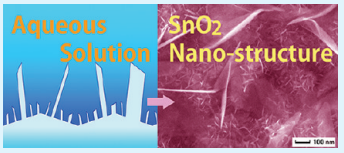

KEYWORDS: *hydrophobic surface, hydrophilic surface, tin oxide, nanosheet, molecular sensor, cancer sensor*

1. INTRODUCTION

Metal oxide nanostructures have been attracting a lot of attention as key materials for future devices. High-temperature annealing has been used to prepare metal oxide particles or particulate films for a long time. However, the annealing caused degradation of nanostructures and device performance.

Recently, an aqueous solution process was developed. Unique nanostructures were fabricated in the solutions.[1−16] Crystal growth was precisely controlled to develop novel nanostructures. The annealing was not required to crystallize metal oxide nanostructures. Additionally, the aqueous solution process had advantages of low energy consumption, low cost of equipment, low manufacturing cost, simple process, and low environmental load. It is attractive as sustainable science and technology.

Hydrophobic surfaces have recently attracted significant attention because of their water-repellency, oil-repellency, antifouling property, antifogging property, self-cleaning property, and the potential applications in various fields.[17−20] Hydrophobic surfaces are found in nature. Leaves of nelumbo nucifera, i.e., sacred lotus, have a self-cleaning property due to their hydrophobic surfaces.[21,22] Water striders walk on water using water-repellent legs.[23,24] Namib desert beetles collect drinking water from fog-laden wind using the hydrophilic/hydrophobic patterned surface of wings.[25] It was reported that maximum water contact angle of a flat surface was below 120°. A combination of nano-/microscaled roughness and hydrophobic materials realized hydropholic surfaces. These indicated that control of nano- and microstructure was important for hydrophobic surfaces. Fluorocarbon layers are widely used for hydrophobic coatings. However, they are less resistant to high temperature. Chemically and thermally stable coatings are required for long-term durability, high-temperature use, and voltage resistance in various applications. Metal oxides are candidate materials for the stable surface coatings. They have high resistance to strong acids, strong alkalis, high temperature of hundreds of degrees Celsius, wear and abrasion, and high electric power. Additionally, the process for fluorocarbon coatings is high cost and difficult to coat on large substrates, complex shapes, particles, tubes, or nanomaterials. A simple and low-cost process is required to be used widely.

Semiconductor metal oxide nanostructures have been fabricated on fluorine-doped tin oxide (FTO) substrates for next generation devices such as molecular sensors, gas sensors, dye-sensitized solar cells, electronic devices, etc. Their semiconductor property, conductivity, transparency, and high surface area are suitable for the devices. Control of hydrophobicity/hydrophilicity and surface modification with functional molecules are required to improve sensitivity and efficiency of the devices.

In this study, we fabricated tin oxide nanosheets on FTO in aqueous solutions without annealing. The hydrophobic surface had water contact angle of 125 degree. It changed to hydrophilic surface with water contact angle of below 1 degree by light irradiation. Moreover, tin oxide nanosheets were modified with dye-labeled monoclonal antibody. They showed strong photoluminescence and high photocurrent. It suggested that they were suitable for electrodes of cancer sensors. A mechanism of cancer sensing was based on photoelectric conversion effect and molecular recognition.

Received: December 21, 2011
Accepted: February 9, 2012
Published: February 9, 2012

   dx.doi.org/10.1021/am201811x | ACS Appl. Mater. Interfaces 2012, 4, 1666−1674

2. EXPERIMENTAL PROCEDURE

2.1. Synthesis of Tin Oxide Nanosheet Coatings on FTO Substrates. The FTO substrate was selected to an initial substrate, since it was suitable to an electrode of a photocurrent conversion type molecular sensor for the following reasons. We were developing the photocurrent conversion type molecular sensor. An electrode was a key for it. It should have high transparency, high conductivity, suitable oxidation-reduction potential and semiconductor property. It should be modified with desired biomolecules for immunological assay or DNA hybridization. Additionally, it should suppress nonspecific adsorption. The FTO substrate had high transparency for excitation light and high electrical conductivity of 9.3−9.7 Ω/□ (Ohms/square). It was suitable to increase photoluminescence and photocurrent. Surface roughness and surface area of the FTO substrate was higher that those of an indium tin oxide (ITO) substrate. They were effective to increase adsorption volume of dye-labeled monoclonal antibody. Electrical conductivity of ITO easily decreased with high temperature treatment, however, FTO had higher heat resistance compared to ITO. Moreover, FTO surface was suitable to grow tin oxide nanostructures, because both of them were SnO_2 crystals. SnO_2 nanocrystals were easily crystallized on SnO_2 crystals of FTO. Surface of FTO should be cleaned completely to realize crystallization of SnO_2 nanocrystals. The FTO substrate was cleaned by decomposition of small amount of adsorbed organic molecules using low wavelength light as follows. Glass substrates coated with transparent conductive FTO films (FTO, SnO_2:F, Asahi glass Co., Ltd., 26 × 50 × 1.1 mm) were blown by air to remove dust and were exposed to a vacuum ultraviolet light for 10 min (VUV, low-pressure mercury lamp PL16-110, air flow, 100 V, 200 W, SEN Lights Co., 14 mW/cm^2 for 184.9 nm at distance from lamp 10 mm, 18 mW/cm^2 for 253.7 nm at distance from lamp 10 mm). The initial FTO substrates showed a water contact angle of 96°. FTO surface, i.e., SnO_2 polycrystal surface, was hydrophilic immediately after preparation in the glass factory. FTO substrates were then covered with paper and stacked to store in air in the factory. Airborne organic molecules and organic molecules on paper adsorbed on the FTO surface. They changed FTO surfaces from hydrophilic to hydrophobic. The surfaces thus showed high water contact angle. The VUV-irradiated surfaces however, were wetted completely (contact angle 0−1°). Various functional groups such as octadecyl or phenyl groups of self-assembled monolayers formed on films are reported to be modified to OH groups by VUV irradiation using low-pressure mercury lamps.[26,27] These suggest that a small amount of adsorbed molecules on the FTO substrates were completely removed by VUV irradiation. Because the original FTO surfaces, i.e., SnO_2 polycrystal surfaces, had hydrophilic OH groups, the original FTO surface covered by hydrophilic OH groups was exposed after the irradiation. The surfaces were modified to hydrophilic with the irradiation. Tin oxide nanosheets were crystallized on the hydrophilic FTO surfaces without organic molecules or contamination at the interface between tin oxide nanosheets and FTO surfaces as follows.

SnF_2 was used as-received (Wako Pure Chemical Industries, Ltd., No. 202-05485, FW: 156.71, purity 90.0%). Distilled water of 200 mL was heated at 94°C in a capped teflon vessel using a drying oven (Yamato Scientific Co., Ltd., DKN402). SnF_2 (870.6 mg) was dissolved in the distilled water at 94°C to be 25 mM. The FTO substrates were immersed in the middle of the solutions with the bottom up, tilted at 15° to the upright. The solutions were heated from 94 to 200 °C for 35 min. Rate of temperature increase was about 3 °C/min. They were kept at 20 0°C for 20 min. The vessels were withdrawn from the oven and naturally cooled for 100 min. The FTO substrates were removed from the solutions. They were cleaned with distilled water and strong air blow. In this procedure, FTO substrates were kept at 200 °C for 20 min as above, but they contacted to the solutions for 155 min in total (35 + 20 + 100 min). Consequently, tin oxide nanosheets were crystallized on the hydrophilic FTO surfaces.

2.2. Surface Modification of Tin Oxide Nanosheets with Prostate Specific Antigen. Prostate specific antigen, i.e., monoclonal antibody of NB013 (anti-human alpha-fetoprotein (AFP) monoclonal antibody, Human-AFPMoAb, No. NB013, IgG1, Nippon Biotest Labo., Tokyo, Japan) was utilized in sensing system because it reacted with human alpha-fetoprotein (AFP) selectively. AFP was not detected from blood serum of a normal adult. However, hepatocellular cancer (hepatocellular carcinoma) and germ cell teratoblastoma as well as hepatic regeneration, viral hepatitis and hepatocirrhosis (cirrhosis) caused increase of AFT concentration. Reaction of monoclonal antibody NB013 with AFP will be used for sensing of hepatocellular cancer. The sensing system can detect human alpha-fetoprotein (AFP) in adult blood serum for early detection of hepatocellular cancer.

Dye of Cy5 was selected because it emitted photoluminescence under excitation of usual red light. Combination of tin oxide semiconductor and dye of cy5 was suitable to generate photocurrent due to oxidation−reduction potential and band gap engineering.

Monoclonal antibody of NB013 was labeled with dye of Cy5. They were dissolved in phosphate buffer solution (PB) of 10 mM (pH7.4). The dye-labeled antibody (Cy5-NB013) is the candidate materials for our newly developed sensor. Cy5 is expected to adsorb on the substrates in the presence of human alpha-fetoprotein (AFP) through antigen-antibody reaction. Red laser of 650 nm (97 mW) was selected since it was suitable for generation of electrons in the combination of dye of Cy5 and semiconductor of SnO_2. Electric signal was created by laser light irradiation on Cy5 at the surface of the electrodes. Generation of photocurrent under the irradiation was an essence of sensing mechanism. Photocurrent conversion system in our sensor is similar to that in a dye-sensitized solar cell. We combined biological reaction of monoclonal antibody NB013 with AFP for sensing of hepatocellular cancer. These are basic principle of our sensor. For comparison, the electrodes covered with antibody that contained no dye were evaluated to measure noise current under irradiation.

Tin oxide nanosheets on FTO substrates were modified with biomolecules as follows. Polyvinyl chloride tape (PVC, CH_2−$CHCl)_n$, 26 × 22 mm, 100 -μm thickness) was perforated with 9 (3 holes × 3 rows) holes 25 mm in diameter using a flatbed cutting plotter (CG-60ST; Mimaki Engineering Co., Ltd.). The middle area of the FTO surfaces were covered with PVC tapes after the deposition of tin oxide nanosheets. Dye-labeled monoclonal antibody (Cy5-NB013) was dissolved in sterile water to be 10 or 1 μg/mL, respectively. Monoclonal antibody (NB013) without dye was dissolved in sterile water to be 10 μg/mL to evaluate noise current, for comparison. Dye-labeled monoclonal antibody solution (Cy5-NB013, 10 μg/mL) of 5 μL was dropped with pipettes onto the 3 holes in the upper row in the PVC tape. Dye-labeled monoclonal antibody solution (Cy5-NB013, 1 μg/mL) of 5 μL or monoclonal antibody solution without dye (NB013, 0 μg/mL) of 5μl was dropped onto the 3 holes in the middle or bottom row, respectively. The substrates were kept at 37 °C for 10 min in air. They were then shaken in distilled water for 10 min using a slide washer (SW-4, Juji Field Inc., Tokyo, Japan).

It was known that hydrophobicity and hydrophilicity affected surface modification for molecular sensors. They were important in developing the sensors. Hdrophobicity and hydropholicity were demonstrated to be controlled in this study. The techniques can be adapted to the needs of desired antigen-antibody reactions. Fortunately, surface modification was not required for our cancer sensor. As-prepared tin oxide nanosheets on the FTO substrates were utilized for surface modification with dye-labeled monoclonal antibody as presented above.

2.3. Characterization. Surface morphology of the substrates was observed with a field-emission scanning electron microscope (FE-SEM; JSM-6335FM, JEOL Ltd.). A part of the substrate was lifted off and thinned to 100 nm in thickness using a focused ion beam (Dual Beam System Nova200, FEI Company, Hillsboro, Oregon, USA). Cross-section images of the substrates were obtained with a transmission electron microscope (TEM; HF-2000, 200 kV, Hitachi). Crystal phase was evaluated with an electron diffraction (ED) that was built into the TEM (HF-2000). An electron beam was channeled into a beam of 30 nm in diameter for ED analysis. Chemical composition was estimated with an energy-dispersive X-ray spectroscopy (EDS) that was built into the TEM (HD-2300A, 200 kV, Hitachi). A resin was used to fix the sample. Oxygen and carbon were detected from the resin with EDS. Chemical composition of the samples was determined with reference to chemical composition of the resin.

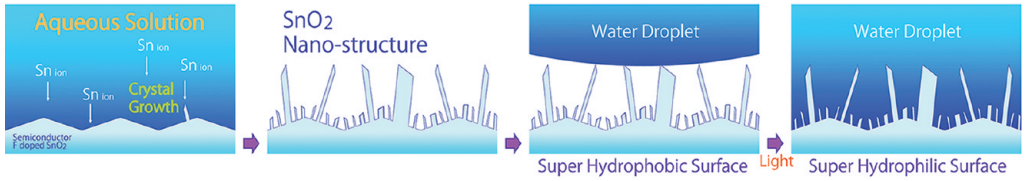

Figure 1. Concept for tin oxide nanosheet coating on a FTO substrate for hydrophobic or hydrophilic surface.

The crystal phase was evaluated with an X-ray diffractometer (XRD; RINT-2100 V, Rigaku) with CuKα radiation (40 kV, 30 mA). The diffraction patterns were analyzed using ICSD (Inorganic Crystal Structure Database) data (FIZ Karlsruhe, Germany and NIST, USA) and FindIt.

Transmittance and reflectance of the substrates were investigated with an ultraviolet−visible spectrophotometer (UV−VIS−NMR; V670, JASCO Co.) with integrating sphere in the wavelength range of 200−800 nm.

Chemical state and chemical composition were analyzed with an X-ray photoelectron spectroscopy (XPS, Kratos analytical, ESCA-3400, Shimazu). The X-ray source (MgKα, 1253.6 eV) was operated at 10 kV and 20 mA. Resolutions for survey analyses or narrow analyses, i.e., FWHM of $Ag3d_{5/2}$ spectrum, were 1.15 eV or 0.95 eV, respectively. Ag was selected for evaluation of spectrum resolution and analysis condition. Since Ag was chemically stable and resistant to oxidation. It showed a sharp $Ag3d_{5/2}$ peak without peaks of oxidized states. Step size (eV) or dwell time (s) for survey analyses or narrow analyses were 1 eV, 150 s or 0.1 eV, 300 s, respectively.

The FTO substrates with tin oxide nanosheets were kept in a plastic case for a month after deposition of tin oxide. Static water contact angle, advancing water contact angle or receding water contact angle were evaluated with a contact angle meter (Easy Drop, DSA20SS, Kruss, Germany). The substrates were exposed to a vacuum ultraviolet light for 10 min. Contact angle was evaluated again after the irradiation.

Surfaces that had a static water contact angle larger than 90° or smaller than 5° were known as hydrophobic or hydrophilic surfaces, respectively. Contact angle was governed by an energy equilibrium and was given by Young equation (eq 1) (see the Supporting Information, Figure S1). Surface chemistry and surface topology influenced the contact angle and contact angle hysteresis. The hysteresis was defined as the difference between the advancing and receding water contact angles. Contact angle measurements gave information about surface properties.

$$\gamma_{ls} = \gamma_{cs} + \gamma_{lc}\cos\theta \quad (1)$$

where γ is interfacial surface energy, θ is contact angle, l is liquid, s is substrate, and c is crystal.

2.4. Evaluation of Photoluminescence and Photocurrent from Tin Oxide Nanosheets with Dye-labeled Prostate Specific Antigen. Tin oxide nanosheets were formed on FTO substrates. They were modified with dye-labeled monoclonal antibody mentioned above. Photoluminescence intensity was evaluated with a Typhoon Trio scanner (GE Healthcare UK Ltd., UK) using an excitation light of 632.8 nm (He/Ne laser). Detection sensitivity was set to PMT 520. Photoelectrochemical experiments were performed in sandwich-type cells. They consisted of the substrate (working electrode), Pt counter electrode and electrolyte solution containing redox pair (I^-/I^{3-}) to fill the cells. Red laser (97 mW with a wavelength of 650 nm) was served as a light source. The photocurrent actions were determined by measuring the short-circuit photocurrents at excitation wavelengths of the red laser. All the measurements were conducted at room temperature. The light was irradiated from a glass side (back side) of the substrates.

3. RESULTS AND DISCUSSION

3.1. Chemistry for Tin Oxide Forming Reaction. SnO_2 is formed though several reaction routes, since tin and other ions formed several complexes and species. A dominant route is shown as follows. Valence of tin ion is shown in equations, because it is important to understand oxidation and formation of tin oxides.[28]

$$Sn(II)F_2 \leftrightarrow Sn(II)^{2+} + 2F^- \quad (2)$$

$$2H_2O \leftrightarrow H_3O^+ + OH^- \quad (3)$$

$$H_2O \leftrightarrow H^+ + OH^- \quad (4)$$

It is known that oxonium-ion is dominant rather than proton in aqueous solutions (eq 3).[28] Proton is, however, used in equations.[29]

$$3Sn(II)^{2+} + 4H_2O \leftrightarrow [Sn(II)_3(OH)_4]^{2+} + 4H^+ \quad (5)$$

$$Sn(II)^{2+} + H_2O \leftrightarrow [Sn(II)(OH)]^+ + H^+ \quad (6)$$

$$2Sn(II)^{2+} + 2H_2O \leftrightarrow [Sn(II)_2(OH)_2]^{2+} + 2H^+ \quad (7)$$

The multinuclear complex of $[Sn(II)_3(OH)_4]^{2+}$ in eq 5 is formed with a small amount of $[Sn(II)(OH)]^+$ in eq 6 and $[Sn(II)_2(OH)_2]^{2+}$ in eq 7.[28]

Multinuclear complex of $[Sn(II)_3(OH)_4]^{2+}$ is circular ion.[28] It is known to be a crystal nucleus of several types of basic tin salts in aqueous solutions at low pH.[28]

SnO_2 or SnO is formed from these complexes. A typical route from $[Sn(II)_3(OH)_4]^{2+}$ is shown as follows.

$$[Sn(II)_3(OH)_4]^{2+} + O_2 \leftrightarrow 3Sn(IV)O_2 + 4H^+ \quad (8)$$

$$[Sn(II)_3(OH)_4]^{2+} + 2H_2O \leftrightarrow 3Sn(IV)O_2 + 8H^+ \quad (9)$$

$$[Sn(II)_3(OH)_4]^{2+} + 2OH^- \leftrightarrow 3Sn(II)O + 3H_2O \quad (10)$$

$$[Sn(II)_3(OH)_4]^{2+} \leftrightarrow 3Sn(II)O + 2H^+ + H_2O \quad (11)$$

Sn^{2+} ion is known to be easily oxidized to Sn^{4+} by dissolved oxygen in the aqueous solutions (eqs 8 and 9).[28] Especially, oxidation of Sn^{2+} ion progresses rapidly in a dilute SnF_2 solution below 0.5 M,[30] because it contains enough oxygen.

SnO is formed from the complex in eqs 10 and 11.

SnO is reported to be oxidized to SnO_2 because of its instability as shown in eqs 12 and 13.[29,31]

$$Sn(II)O + H_2O \leftrightarrow Sn(IV)O_2 + H_2 \quad (12)$$

$$2Sn(II)O + O_2 \leftrightarrow 2Sn(IV)O_2 \quad (13)$$

Moreover, SnO_2 or SnO is formed from $[Sn(II)(OH)]^+$ in eq 6 or $[Sn(II)_2(OH)_2]^{2+}$ in eq 7 similarly.

Generation of gas was observed immediately after addition of SnF_2 in water at 90°C. The solutions were kept at 200°C for 20 min. Ion concentration, balance of ions and pH changed during synthesis period. They affected formation of SnO_2. After having

been immersed in the solutions, the substrates were rinsed under running water and dried with a strong air spray. The nanosheets were not removed under running water or with air spray. Direct crystallization of tin oxide on the substrates caused high adhesion strength, which was required for sensors or solar cells. Fluorine ions were doped in tin oxide nanosheets. Fluorine doping was known to be effective for performance advances of sensors or solar cells.[32] Residual fluorine ions remained in the solutions.

3.2. Morphology, Crystal Structure, and Chemical Composition of a Tin Oxide Nanosheet Coating on a FTO Substrate. Tin oxide nanosheets were formed on FTO substrates in aqueous solutions (Figure 1). Initial FTO substrates had surface relief structures of about 500 nm to 1000 nm. Since they were polycrystals of SnO_2. Surface of them were covered with tin oxide nanosheets uniformly (Figure 2a). They consisted of two kinds of crystals (Figure 2b). Larger nanosheets were about 100−500 nm in plane size and about 10−50 nm in thickness (Figure 2b). Smaller crystals were about 10−100 nm in plane size and about 1−10 nm in thickness (Figure 2c). Aspect ratio of them was roughly estimated to 10. Anisotropic crystal growth allowed us to synthesize tin oxide nanosheet.

Cross-section images of tin oxide nanosheets were observed with the TEM. The FTO layer of 800-900 nm in thickness was observed on a glass substrate (Figure 3e). Tin oxide nanosheets were deposited on the FTO layer (Figure 3a). Large nanosheet that was about 300 nm in plane size and about 20 nm in thickness was observed on the surface. Aspect ratio was roughly estimated to about 15 (300 nm/20 nm). It stood perpendicular to the substrate with a tilted angle of about 10°. Electron diffraction pattern was obtained from the nanosheet in area 1 (Figure 3a, area 1). It was assigned to single phase of SnO_2 crystal without any additional phase. The pattern was not diffraction rings but electron diffraction spots. It indicated that the nanosheet was a single crystal. Crystal lattice distance that was parallel to SnO_2 110 crystal planes was estimated to 0.346 nm. Both of crystal lattice distances that were parallel to SnO_2 101 or 011 were estimated to 0.293 nm. They were same lattice distance because SnO_2 had a tetragonal crystal system that had *a*-axis, *a*-axis, and *c*-axis. Chemical composition of the nanosheet was estimated to Sn:O = 1:1.8 with the EDS analysis system. It was similar to chemical composition of SnO_2 rather than SnO.

Nanosheets in area 2 or 3 (Figure 3b, c) showed electron diffraction patterns. They were assigned to single phase of SnO_2. Some nanosheets were included in evaluation areas. Therefore, electron diffraction patterns had a few diffraction spots for each lattice distance. Two diffraction spots were, for instance, assigned to 110 of SnO_2 in diffraction pattern from area 2. It suggested that two single crystals of SnO_2 were included in area 2. Crystal lattice distance of SnO_2 110 was estimated to 0.340 nm. Those of SnO_2 211 or 221 were 0.182 or 0.149 nm, respectively. Electron diffraction pattern from area 3 was also assigned to single phase of SnO_2 with some spots for each lattice distance. Crystal lattice distance of SnO_2 110, 211, or 221 was estimated to be 0.346, 0.182, or 0.146 nm, respectively. Chemical composition in area 2 or 3 was estimated to be Sn:O = 1:2.6. It was larger than that of SnO_2. Oxygen and carbon were detected from the resin over coat which was used to fix the substrate for thinning process and TEM observation (Figure 3a, area 4). The resin was included in area 2 or 3. It increased amount of oxygen in EDS analysis.

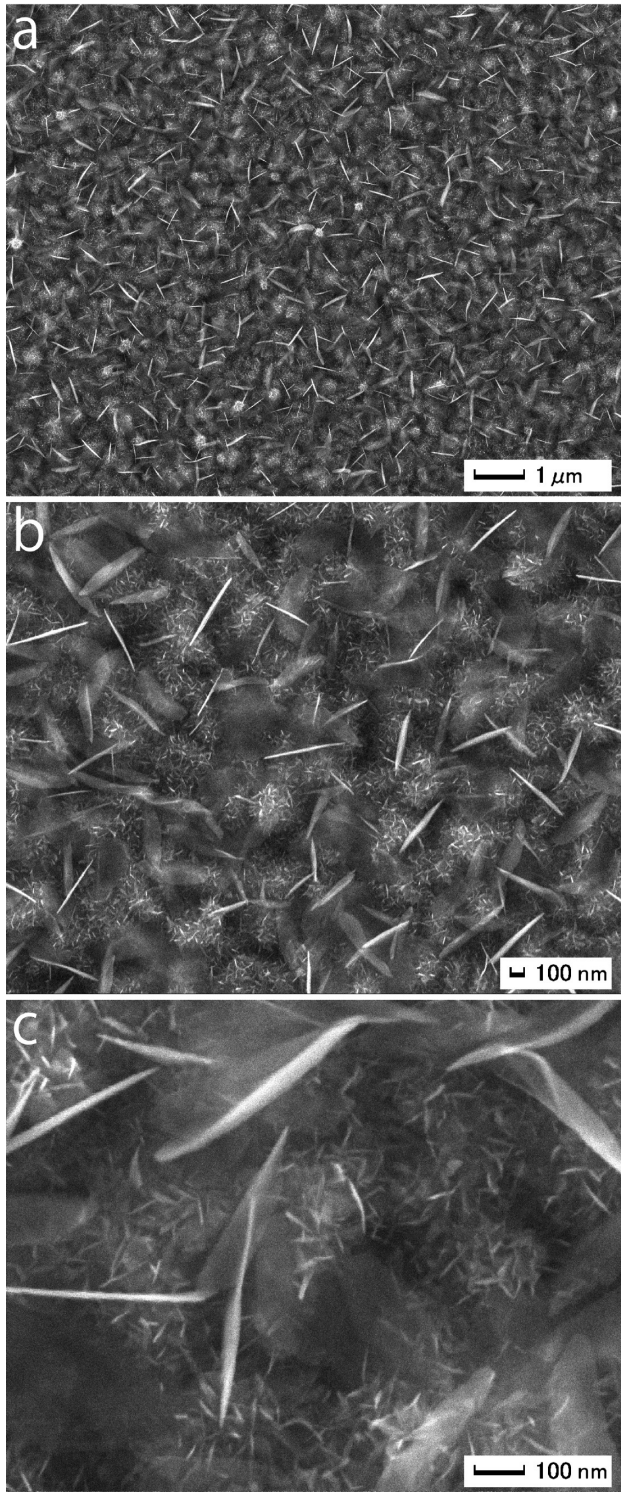

Figure 2. (a) Surface morphology of a tin oxide nanosheet coating on a FTO substrate. (b, c) Magnified area of a.

Crystal growth direction of the nanosheet was shown in Figure 3a. Two diffraction spots of SnO_2 110 were clearly observed in an electron diffraction pattern. The pattern was obtained from electron diffraction evaluation area 1. It indicated that the direction of *a*-axis was inclined at an angle of about 35° from perpendicular to the substrate. Longer direction of the tin oxide nanosheet in area 1 was also inclined at a similar angle from perpendicular to the substrate. They suggested that longer

dx.doi.org/10.1021/am201811x | ACS Appl. Mater. Interfaces 2012, 4, 1666−1674

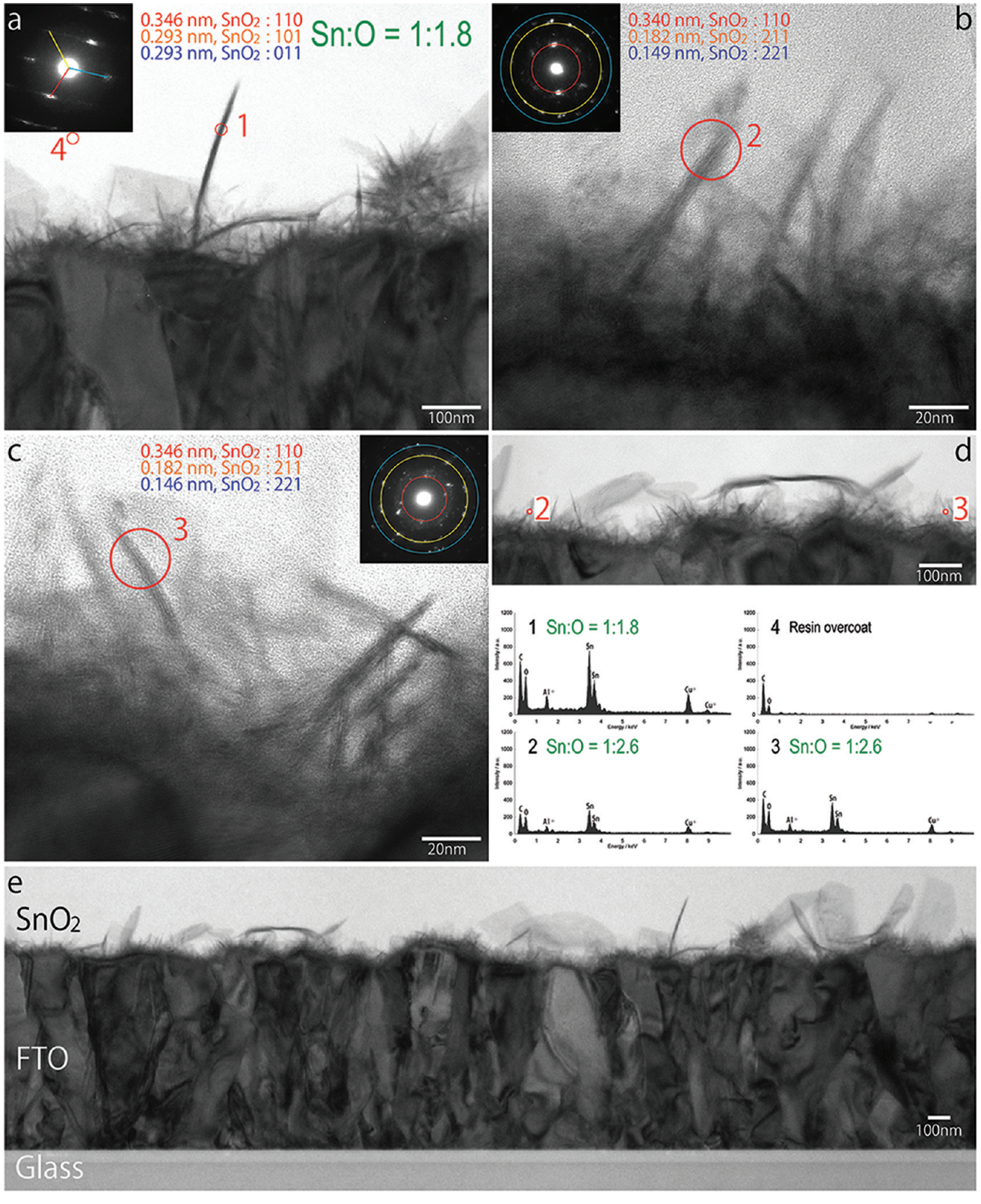

Figure 3. Cross-section images, electron diffractions, and chemical ratio of a tin oxide nanosheet coating on a FTO substrate. (a–d) Magnified area of image e.

direction of the tin oxide nanosheet, i.e., in-plane direction of the tin oxide nanosheet, was same to direction of *a*-axis. SnO_2 had tetragonal crystal structure that had *a*-axis, *a*-axis and *c*-axis. SnO_2 grew along not *c*-axis but *a*-axis to form sheet structure. Several nanosheets overlapped in other evaluation areas (Figure3b, area 2; Figure3c, area 3). Crystal growth direction was difficult to be analyzed in these points.

3.3. XPS Analysis of a Tin Oxide Nanosheet Coating on a FTO Substrate. Tin, oxygen, fluorine, and carbon were detected from the surface of tin oxide nanosheet coating with

dx.doi.org/10.1021/am201811x | *ACS Appl. Mater. Interfaces* 2012, 4, 1666–1674

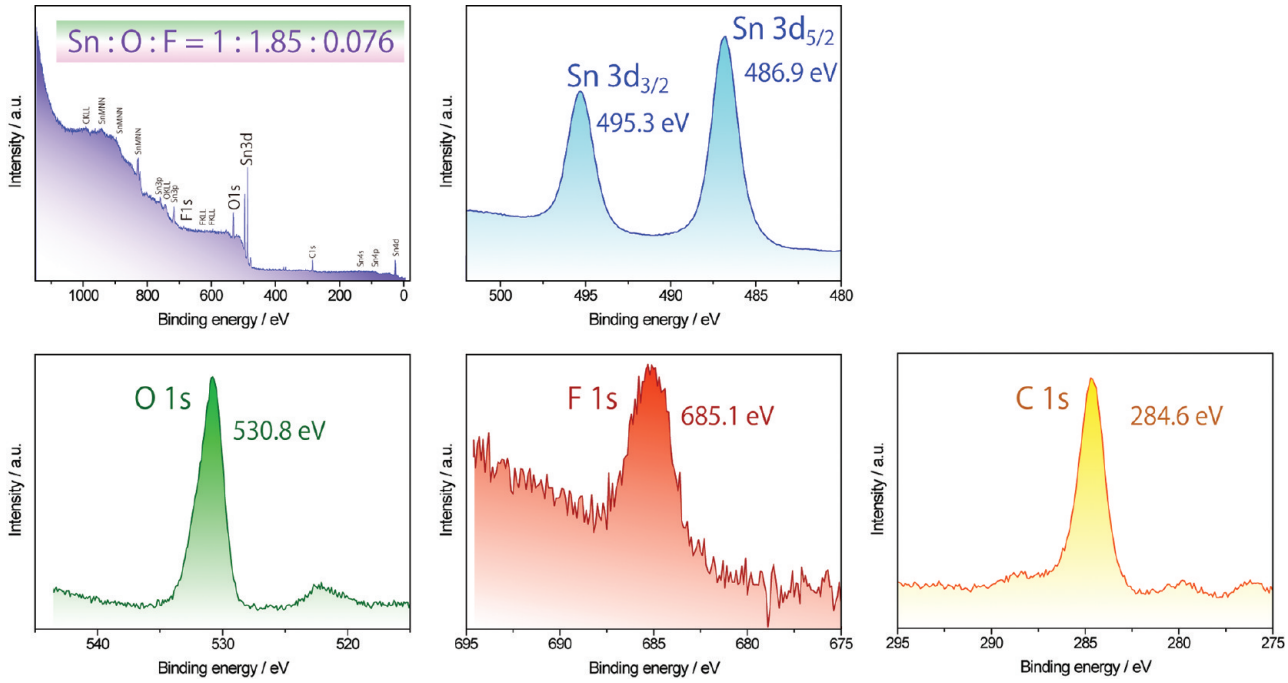

Figure 4. XPS spectra of survey, tin, oxygen, fluorine, or carbon for a tin oxide nanosheet coating on a FTO substrate.

XPS analysis (Figure 4). Sn $3d_{5/2}$, $Sn3d_{3/2}$, O 1s, F 1s, and C 1s spectra were evaluated in detail. Chemical composition was estimated to Sn:O = 1:1.85. It was similar to chemical composition of SnO_2 rather than SnO. It was consistent with EDS analysis in TEM observation. Sn $3d_{5/2}$ or $Sn3d_{3/2}$ spectra were observed at 486.9 or 495.3 eV, respectively. Binding energy of Sn $3d_{5/2}$ was similar to that of Sn^{4+} in SnO_2 (486.6 eV[33]), and higher than that of Sn^{2+} in SnO (485.9 eV[33]) or Sn metal (484.8,[34] 484.85,[35] 484.87,[36] 484.9,[37] and 485.0 eV[38]). It suggested that tin ions were positively charged by forming direct bonds with oxygen ions.

Binding energy of O 1s was 530.8 eV. It was similar to that in SnO_2 (530.5 eV[33]), in which O ions connected to Sn^{4+} ions, and higher than that in SnO (529.8 eV[33]), in which O ions connected to Sn^{2+} ions. Sn $3d_{5/2}$ and O 1s spectra indicated that nanosheets were SnO_2 rather than SnO or Sn metals.

F 1s spectrum was observed at 685.1 eV. The binding energy was similar to that of fluorine ions which were doped in tin oxide (684.4 eV[39]). It suggested that fluorine ions were doped in the nanosheets. Chemical composition was estimated to Sn:F = 1:0.076. It was known that fluorine doping of about 0.03−0.1 was effective to improve conductivity of tin oxide.[32] Tin oxide nanostructures with high conductivity were strongly required for sensors and dye-sensitized solar cells.

Carbon was detected from the surface due to surface contamination. All spectra were corrected using standard binding energy of C−C bonds (C 1s, 284.6 eV) in surface contaminations.

3.4. X-ray Diffraction from a Tin Oxide Nanosheet Coating on a FTO Substrate. The tin oxide nanosheet coating on the FTO substrate showed x-ray diffraction peaks at 2θ = 26.5, 33.8, 37.8, 38.9, 42.6, 51.6, 54.6, 61.7, 64.6, 65.8, 71.1, 78.4, 80.8, 83.4, 89.5, 90.6, 92.9, or 107.9° (Figure 5). They were assigned to diffractions from 110, 101, 200, 111, 210, 211, 220, 310, 112, 301, 202, 321, 400, 222, 312, 411, 420, or 213 crystal planes, respectively. X-ray diffraction data of JCPDS No. 41-1445 (SnO_2) was used for identification. The

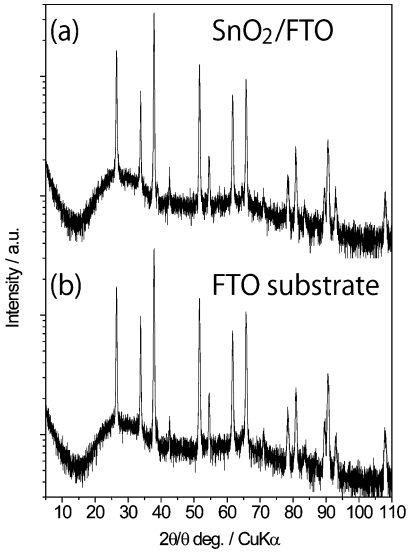

Figure 5. X-ray diffraction patterns of (a) a tin oxide nanosheet coating on a FTO substrate or (b) a bare FTO substrate.

diffractions were also observed from a bare FTO substrate, and were assigned to SnO_2. Clear distinction was not observed between the XRD patterns, because the tin oxide nanosheet coating was a thin layer, and both the tin oxide nanosheet coating and the FTO substrate were SnO_2.

3.5. Transparency of a Tin Oxide Nanosheet Coating on a FTO Substrate. The bare FTO substrate showed transmittance of 72.0, 78.8 , 78.2, 77.4, or 76.4% at 400, 500, 600, 700, or 800 nm, respectively (Figure 6). Transmittance increased by tin oxide nanosheet coating to 72.3, 81.6, 82.8, 83.4 or 82.8% at 400 , 500, 600, 700, or 800 nm, respectively. The increase in transmittance was explainable in terms of reflectance. Reflectance of the bare FTO substrate was 14.3, 11.4, 12.6, 12.0, or 11.0% at 400, 500, 600, 700 or 800 nm, respectively. It decreased by tin oxide nanosheet coating to

dx.doi.org/10.1021/am201811x | ACS Appl. Mater. Interfaces 2012, 4, 1666−1674

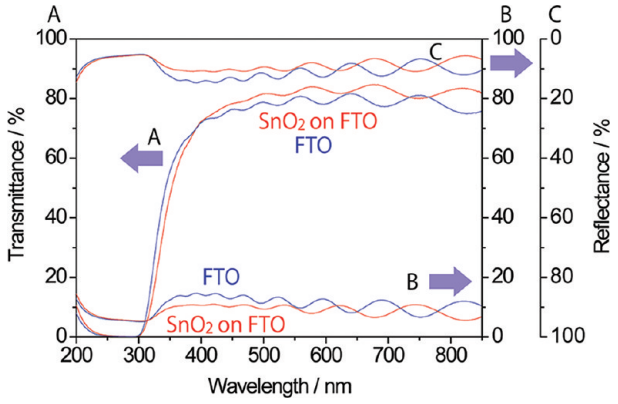

Figure 6. (A) Optical transmittance and (B, C) reflectance of (red) a tin oxide nanosheet coating on a FTO substrate or (blue) a bare FTO substrate.

10.6, 9.3, 9.3, 7.7, or 6.6% at 400, 500, 600, 700, or 800 nm, respectively. It indicated that the tin oxide nanosheet coating had antireflection effect. The decrease of reflectance caused the increase of transmittance. The tin oxide nanosheet coating can be used for an antireflection coating.

3.6. Hydrophobicity of a Tin Oxide Nanosheet Coating on a FTO Substrate. Static water contact angle of the tin oxide nanosheet coating on the FTO substrate was 125°. Advancing contact angle and receding contact angle were 140 or 120°, respectively. The surface showed hydrophobicity for the following reasons. The FTO substrates with tin oxide nanosheets were kept in a plastic case for a month after deposition of tin oxide. Slight amount of airborne organic molecules adsorbed on the surface. The coatings had micro-sized and nano-sized structures. It is well-known that micro- and nanostructures enhance hydrophobicity of an original hydrophobic surface. Hydrophobicity of 125° was realized by combination of slight amount of airborne organic molecules and micro/nanostructures.

Tin oxide is quite resistant to high temperature up to several hundred degrees, oxidation, acid, base, organic solvent, salt water, or sunlight because it is oxidized metal. Tin oxide nanosheet coatings were formed on FTO substrates at 90°C in aqueous solutions. The coatings can be formed on various materials such as metals, polymers, papers and biomaterials. Additionally, uniformity of the coating was one of the advantages of a simple immersion process. The coatings can be formed on not only flat substrates, but also nanosized materials, particles, fibers, meshes, tubes, complex shape structures, medical equipments, automobile windshields, or ship's fulls.

High hydrophobicity was realized by adsorption of slight amount of airborne organic molecules. It indicated that thin organic molecular layers were effective to modify tin oxide surfaces. Recently, artificial thin organic molecular layers, i.e., self-assembled monolayers (SAMs), have been reported.[40−43] Surfaces of metal oxides, glasses or silicons were modified with SAMs of octadecyl groups to hydrophobic surfaces.[1,44,45] SAMs can be applied to the tin oxide nanosheet coating on a FTO substrate instead of adsorbed organic molecules. It would improve controllability of surface modification.

(7). Hydrophilicity of a Tin oxide Nanosheet Coating on a FTO Substrate. The coating was irradiated with VUV light for 10 min in air. Ozone was generated from oxygen gas

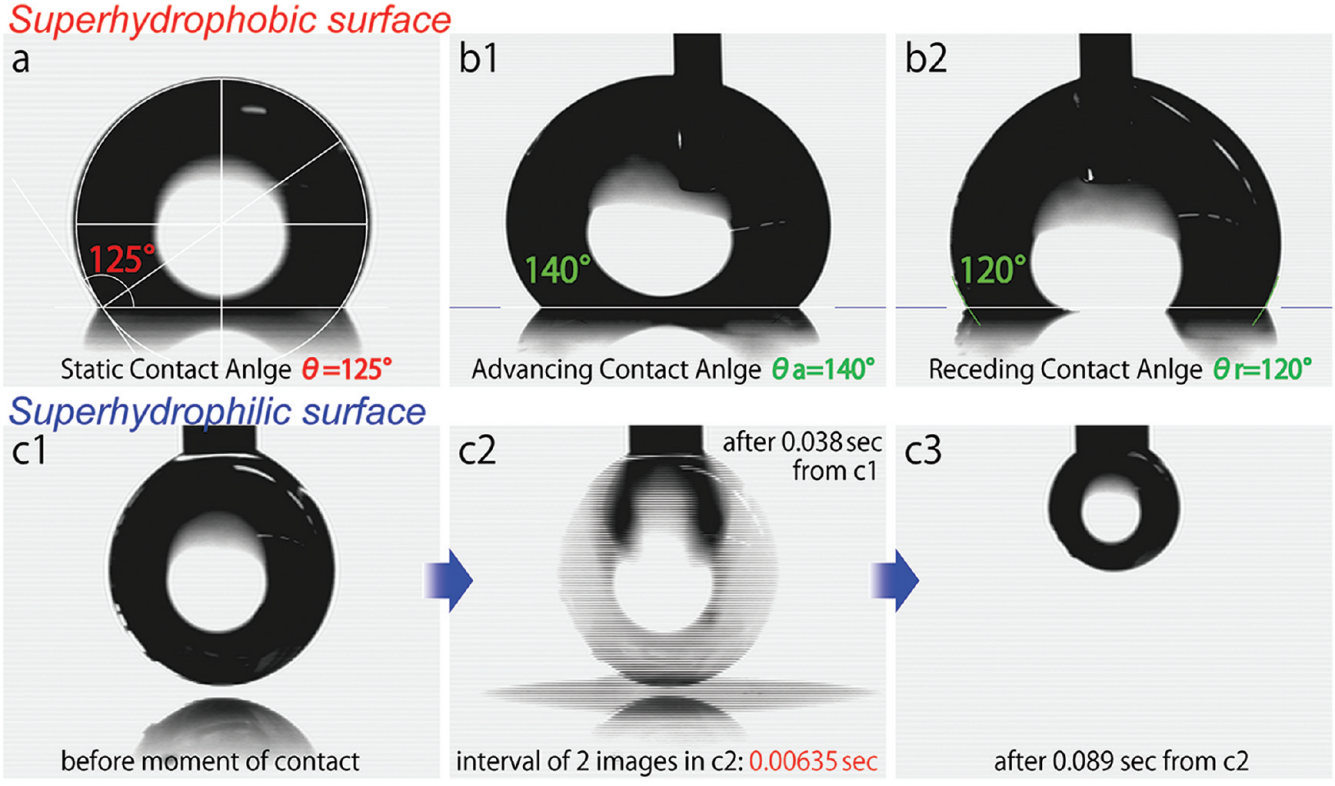

Figure 7. Water contact angle of a tin oxide nanosheet coating on a FTO substrate. (a) Static contact angle, (b1) advancing contact angle, (b2) receding contact angle of hydrophobic surface. (c1−3) High-speed movie of rapid spread of a water droplet on hydrophilic surface after light irradiation.

dx.doi.org/10.1021/am201811x | ACS Appl. Mater. Interfaces 2012, 4, 1666−1674

by the irradiation. Strong light energy and ozone broke chemical bonds and decomposed adhered organic molecules on the surfaces of tin oxide nanosheets. Consequently, the surfaces changed to hydrophilic by the irradiation. Static water contact angle was below detection limit of 1 degree. A water droplet was shown above the surface before the moment of the contact (Figure 7c1). It rapidly spread on the hydrophilic surface (Figure 7c2). The droplet was not observed after the moment of contact (Figure 7c3). The photograph (Figure 7c2) was a composite image that consisted of two captured images. Two different images were shown in Figure 7c2, because of rapid shape change of the droplet. Interval of two images in Figure 7c2 was 0.00635 s. It indicated that the droplet spread on the surface in less than 0.00635 sec. The droplet spread rapidly because the surface was hydrophilic. The size change of the droplet was further estimated. The droplet of 2 μL contacted the surface. One microliter of water remained at the tip of a needle. One microliter (= 1 mm^3) of water spread on the surface. The droplet was spread to a disk-shaped water layer. It was about 10 mm in diameter. Thickness, i.e., height, of the water layer was estimated to 25μm using a model of a spherical crown (spherical sector, spherical segment of one base) (see Figure S1 in the Supporting Information) and eq 1. It indicated that the droplet spread widely to form a very thin water layer.

$$V = \frac{\pi h}{6}(3r^3 + h^2) \tag{14}$$

where V is volume of a water layer, 1 mm^3 (1 μL), r is radius of a water layer, 5 mm, and h is height of a water layer (mm).

Hydrophilicity is known to be enhanced by surface asperity. The tin oxide nanosheet coating on the FTO substrate had both large nanosheets 100−500 nm in plane size and small nanosheets 10−100 nm in plane size. Combination of them increased surface asperity and improved surface area. The unique surface structure contributed high hydrophilicity.

(8). Photoluminescence and Photocurrent from Tin Oxide Nanosheets with dye-Labeled Prostate Specific Antigen. The tin oxide nanosheets with dye-labeled prostate specific antigen (10ug/mL) showed strong photoluminescence. It was 2600× the luminescence from the tin oxide nanosheets with unlabeled prostate specific antigen (Table1, P.L.). It was 4× the luminescence from the tin oxide nanosheets with dye-labeled prostate specific antigen (1ug/mL) (Table1, P.L.). It indicated that photoluminescence drastically increased by surface modification with dye-labeled prostate specific antigen.

Table 1. Photoluminescence and Photocurrent from a Tin Oxide Nanosheet Coating on a FTO Substrate Modified with (A) Dye-Labeled Prostate Specific Antigen (Cy5-NB013) of 10 μg/mL, (B) Dye-Labeled Prostate Specific Antigen (Cy5-NB013) of 1 μg/mL, or (C) Unlabeled Prostate Specific Antigen (NB013) of 10 μg/mL under Excitation Light

surface modification[a]	P.L. (a.u.)[b]	P.C. (nA)[c]
(A) 10 μg/mL Cy5-NB013	3474216	604
(B) 1 μg/mL Cy5-NB013	878252	303
(C) 10 μg/mL NB013	1336	327
signal to noise ratio, A/C	2600	2

[a](A) 10 μg/mL Cy5-NB013: dye-labeled prostate specific antigen. (B) 1 μg/mL Cy5-NB013: dye-labeled prostate specific antigen. (C) 10 μg/mL NB013: unlabeled prostate specific antigen. [b]P.L.: Photoluminescence under excitation light of 632.8 nm. [c]P.C.: Photocurrent under excitation light of 650 nm, 97 mW.

Photocurrent was successfully generated from the tin oxide nanosheets with dye-labeled prostate specific antigen (monoclonal antibody of NB013, 10ug/mL Cy5-NB013). It reached 603.7 nA under irradiation of red light (97 mW, 650 nm) (Table1 P.C., A). It indicated that photon energy was converted to electrical current by the combination of semiconductor tin oxide and dye on the surface of the tin oxide nanosheets. Photoelectric conversion effect will be used for molecular sensing. Additionally, it was demonstrated that prostate specific antigen of monoclonal antibody of NB013 was applicable to the photocurrent conversion sensing system. Influence of dye-labeled prostate specific antigen concentration was further evaluated in details. The tin oxide nanosheets with dye-labeled prostate specific antigen of 1 μg/mL or with unlabeled prostate specific antigen showed photocurrent of 303.0 or 327.3 nA, respectively (Table1 P.C., (B, C)). They were mainly caused from a noise current in a device. The signal to noise ratio was estimated to about 2 (= 603.7 nA/327.3 nA) from these measurements. The tin oxide nanosheets with dye-labeled prostate specific antigen will be used for electrodes in prostate cancer sensors.

The FTO substrates were modified with tin oxide nanoparticulate films or thin nanoparticle layers for comparison. However, photoluminescence and photocurrent were not improved well. Photoluminescence related with adsorbed amount of dye-labeled protein. High surface area was required to increase adsorbed amount. Size of open pores should be larger than that of the dye-labeled protein. The nanoparticulate films didn't have enough volume of open pores which were suitable for adsorption of dye-labeled proteins. Thin nanoparticle layers didn't increase surface area drastically. Photocurrent related with adsorbed amount of dye-labeled protein and electrical conductivity. The nanoparticulate films had many grain boundaries in the films. They decreased electrical conductivity and photocurrent. Sheet structure was one of the most effective morphologies for the sensor. Two-dimensional sheet structure had high surface area per unit weight. The sheet assembly formed suitable open spaces between the sheets. They were larger than dye-labeled proteins. The sheet had no grain boundaries inside. The sheet stood perpendicular to the FTO substrate. It formed on the FTO directly without intermediate layers or particulate layers. These contributed high surface area, suitable size of open pores, and high electrical conductivity.

4. CONCLUSION

We developed nanostructured hydrophobic surface coatings and hydrophilic surface coatings. FTO substrates were coated with the tin oxide nanosheets by simple immersion into aqueous solutions. SnO_2 nanosheets were crystallized on FTO substrates to modify the surfaces. The surface coatings were fluorine doped tin dioxide nanosheets with chemical ratio of Sn : O : F = 1:1.85:0.076. Transparency of the substrates was improved by the surface coating due to suppression of surface diffuse reflection. The advancing, receding or static water contact angles of the surface coatings were 140°, 120°, or 125°, respectively. Water contact angle hysteresis was 20°. Hydrophobic surface was modified to hydrophilic surface of static water contact angle below 1° by simple irradiation of low pressure mercury lamp in air. The easy low-cost procedure can be applied to hydrophobic surface coating or hydrophilic

surface coatings of various kinds of materials including metals, glasses, polymers, papers, and biomaterials.

Furthermore, the tin oxide nanosheet coatings on the FTO substrates were modified with dye-labeled monoclonal antibody. Monoclonal antibody reacts with human alpha-fetoprotein in blood serum of hepatocellular cancer patient. Photoluminescence and photocurrent were detected from the substrates under excitation of red light. Photoluminescence was 2600 times of that from the tin oxide nanosheets with unlabeled prostate specific antigen. Photocurrent reached to 603.7 nA to indicate high ability of photocurrent conversion system. Combination of tin oxide semiconductor and dye was suitable for the system. Reaction of monoclonal antibody with alpha-fetoprotein can be used for detection mechanism. The photocurrent conversion system will open the door for cancer sensing.

■ ASSOCIATED CONTENT

Ⓢ Supporting Information

Model of a droplet for estimation of height is included. This material is available free of charge via the Internet at http://pubs.acs.org/.

■ AUTHOR INFORMATION

Corresponding Author

*E-mail: masuda-y@aist.go.jp.

Notes

The authors declare no competing financial interest.

■ ACKNOWLEDGMENTS

The authors thank Dr. Shuji Sonezaki, Dr. Hitoshi Ohara, Dr. Makoto Bekki, Dr. Yoshimasa Yamana, and Dr. Masako Ajimi of TOTO Ltd. Research Laboratory. This work was partially supported by METI, Japan, as part of R&D for High Sensitivity Environment Sensor Components.

■ REFERENCES

(1) Masuda, Y.; Kinoshita, N.; Sato, F.; Koumoto, K. *Cryst. Growth Des.* **2006**, *6*, 75−78.
(2) Xiang, J. H.; Masuda, Y.; Koumoto, K. *Adv. Mater.* **2004**, *16*, 1461−1464.
(3) Masuda, Y.; Ohji, T.; Kato, K. *Cryst. Growth Des.* **2010**, *10*, 913−922.
(4) Chu, D. W.; Masuda, Y.; Ohji, T.; Kato, K. *Langmuir* **2010**, *26*, 2811−2815.
(5) Hu, X. L.; Masuda, Y.; Ohji, T.; Kato, K. *Cryst. Growth Des.* **2010**, *10*, 626−631.
(6) Masuda, Y.; Kato, K. *Cryst. Growth Des.* **2009**, *9*, 3083−3088.
(7) Hu, X. L.; Masuda, Y.; Ohji, T.; Kato, K. *Cryst. Growth Des.* **2009**, *9*, 3598−3602.
(8) Chu, D. W.; Zeng, Y. P.; Jiang, D. L.; Masuda, Y. *Sens. Actuators, B* **2009**, *137*, 630−636.
(9) Masuda, Y.; Kato, K. *Chem. Mater.* **2008**, *20*, 1057−1063.
(10) Masuda, Y.; Ohji, T.; Kato, K. *Eur. J. Inorg. Chem.* **2011**, 2819−2825.
(11) Masuda, Y.; Kato, K. *Cryst. Growth Des.* **2008**, *8*, 3213−3218.
(12) Masuda, Y.; Kato, K. *Cryst. Growth Des.* **2008**, *8*, 275−279.
(13) Masuda, Y.; Kato, K. *Cryst. Growth Des.* **2008**, *8*, 2633−2637.
(14) Tsukuma, K.; Akiyama, T.; Imai, H. *J. Non-Cryst. Solids* **1997**, *210*, 48−54.
(15) Shirahata, N.; Yokogawa, Y.; Kameyama, T.; Hozumi, A. *J. Vac. Sci. Technol., A* **2004**, *22*, 1734−1738.
(16) Ohgi, H.; Maeda, T.; Fujihara, S.; Imai, H. *Chem. Lett.* **2004**, *33*, 738−739.
(17) Nosonovsky, M.; Bhushan, B. *Multiscale Dissipative Mechanisms and Hierarchical Surfaces: Friction, Superhydrophobicity, and Biomimetics*; Springer-Verlag: Heidelberg, Germany, 2008.
(18) Bhushan, B.; Jung, Y. C.; Koch, K. *Philos. Trans. R. Soc. London, Ser. A* **2009**, *367*, 1631−1672.
(19) Bhushan, B.; Jung, Y. C. *Prog. Mater. Sci.*, **2011**, *56*, 1−108.
(20) Bhushan, B. *Beilstein J. Nanotechnol.* **2011**, *2*, 66−84.
(21) Barthlott, W.; Neinhuis, C. *Planta* **1997**, *202*, 1−8.
(22) Cheng, Y. T.; Rodak, D. E.; Wong, C. A.; Hayden, C. A. *Nanotechnology* **2006**, *17*, 1359−1362.
(23) Gao, X. F.; Jiang, L. *Nature* **2004**, *432*, 36−36.
(24) Shi, F.; Niu, J.; Liu, J. L.; Liu, F.; Wang, Z. Q.; Feng, X. Q.; Zhang, X. *Adv. Mater.* **2007**, *19*, 2257−2261.
(25) Zhai, L.; Berg, M. C.; Cebeci, F. C.; Kim, Y.; Milwid, J. M.; Rubner, M. F.; Cohen, R. E. *Nano Lett.* **2006**, *6*, 1213−1217.
(26) Dressick, W. J.; Calvert, J. M. *Jpn. J. Appl. Phys.* **1993**, *32*, 5829−5839.
(27) Dressick, W. J.; Dulcey, C. S.; Georger, J. H.; Calvert, J. M. *Chem. Mater.* **1993**, *5*, 148−150.
(28) F. Albert Cotton, G. W., Paul L. Gaus *Basic Inorganic Chemistry*, 3rd ed.; John Wiley & Sons: New York, 1995.
(29) Ararat Ibarguena, C.; Mosqueraa, A.; Parrab, R.; Castrob, M. S.; Rodríguez-Páeza, J. E. *Mater. Chem. Phys.* **2007**, *101*, 433−440.
(30) Denes, G.; Lazanas, G. *Hyperfine Interact.* **1994**, *90*, 435−439.
(31) Baes, C. F.; Mesiner, R. E. *The Hydrolysis of Cations*; John Wiley & Sons: New York, 1976.
(32) Han, C. H.; Han, S. D.; Singh, I.; Toupance, T. *Sens. Actuators, B* **2005**, *109*, 264−269.
(33) Kwoka, M.; Ottaviano, L.; Passacantando, M.; Santucci, S.; Czempik, G.; Szuber, J. *Thin Solid Films* **2005**, *490*, 36−42.
(34) Parry-Jones, A. C.; Weightman, P.; Andrews, P. T. *J. Phys. C: Solid State Phys.* **1979**, *12*, 1587−1600.
(35) Wagner, C. D.; Riggs, W. M.; Davis, L. E.; Moulder, J. F.; Muilenberg, G. E. *Handbook of X-ray Photoelectron Spectroscopy*; Perkin-Elmer Corp.: Eden Prairie, MN, 1979.
(36) Pessa, M.; Vuoristo, A.; Vulli, M.; Aksela, S.; Väyrynen, J.; Rantala, T.; Aksela, H. *Phys. Rev. B: Condens. Matter Mater. Phys.* **1979**, *20*, 3115−3123.
(37) Lin, A. W. C.; Armstrong, N. R.; Kuwana, T. *Anal. Chem.* **1977**, *49*, 1228−1235.
(38) Wagner, C. D. *Faraday Discuss.* **1975**, *60*, 291−318.
(39) Martinez, A. I.; Huerta, L.; de Leon, J.; Acosta, D.; Malik, O.; Aguilar, M. *J. Phys. D: Appl. Phys.* **2006**, *39*, 5091−5096.
(40) Masuda, Y.; Kondo, M.; Koumoto, K. *Cryst. Growth Des.* **2009**, *9*, 555−561.
(41) Masuda, Y.; Yamagishi, M.; Koumoto, K. *Chem. Mater.* **2007**, *19*, 1002−1008.
(42) Sawada, S.; Masuda, Y.; Zhu, P. X.; Koumoto, K. *Langmuir* **2006**, *22*, 332−337.
(43) Masuda, Y.; Itoh, T.; Koumoto, K. *Adv. Mater.* **2005**, *17*, 841−845.
(44) Masuda, Y.; Itoh, T.; Koumoto, K. *Langmuir* **2005**, *21*, 4478−4481.
(45) Masuda, Y.; Itoh, T.; Itoh, M.; Koumoto, K. *Langmuir* **2004**, *20*, 5588−5592.